Article

Not peer-reviewed version

(H-DIR)^2: A Scalable Entropy-Based Framework for Anomaly Detection and Cybersecurity in Cloud IoT Data Centers

Davide Tosi *,‡ and Roberto Pazzi *,‡

Posted Date: 22 May 2025

doi: 10.20944/preprints202505.1716.v1

Keywords: hybrid distributed information retrieval; entropy-based anomaly detection; associated random neural network; RDF/SPARQL explainability; cloud–IoT security; sub-second detection latency; semantic-adaptive cyber defense

(H-DIR)^2: A Scalable Entropy-Based Framework for Anomaly Detection and Cybersecurity in Cloud IoT Data Centers

Davide Tosi *,‡ **and Roberto Pazzi** *,‡

Universite gli Studi dell'Insubria, Varese, Italy

* Correspondence: davide.tosi@uninsubria.it, roberto.pazzi@uninsubria.it; Tel.: +39.0332.219988

‡ These authors contributed equally to this work.

Abstract: Modern cloud–IoT infrastructures face increasingly sophisticated and diverse cyber threats that challenge traditional detection systems in terms of scalability, adaptability, and explainability. In this paper, we introduce (H-DIR)^2, a hybrid entropy-based framework designed to detect and mitigate anomalies in large-scale, heterogeneous networks. The framework combines Shannon entropy analysis with Associated Random Neural Networks (ARNN) and integrates semantic reasoning through RDF/SPARQL, all embedded within a distributed Apache Spark pipeline.We validate (H-DIR)^2 on three critical attack scenarios—SYN Flood (TCP), DAO–DIO (RPL), and NTP amplification (UDP)—using real-world datasets. The system achieves a mean detection latency of 247 ms and an AUC of 0.978 for SYN Floods. For DAO–DIO manipulations, it increases packet delivery ratio from 81.2% to 96.4% ($p < 0.01$), and for NTP amplification, it reduces peak load by 88%. The framework scales vertically to millions of endpoints and horizontally across datasets exceeding 10 TB.All code, datasets, and Docker images are publicly released to support full reproducibility. By coupling adaptive neural inference with semantic explainability, (H-DIR)^2 provides a scalable and transparent approach to cloud–IoT cybersecurity, establishing a baseline for future developments in edge-aware and zero-day threat detection.

Keywords: hybrid distributed information retrieval; entropy-based anomaly detection; associated random neural network; RDF/SPARQL explainability; cloud–IoT security; sub-second detection latency; semantic-adaptive cyber defense

1. Introduction

Modern cloud–IoT infrastructures are increasingly vulnerable to sophisticated protocol-level threats, ranging from volumetric attacks such as TCP SYN floods to semantic manipulations of routing protocols. Recent studies emphasize the importance of monitoring the expected behavior of IoT devices and implementing advanced security mechanisms to detect and mitigate such attacks. [9]

To tackle this heterogeneity, we propose the *Hybrid–Dynamic Information Risk* framework, (H–DIR)^2, which fuses a Hybrid Distributed Information Retrieval (H–DIR) architecture [24] with dynamic, entropy-driven risk mitigation.

The Hybrid Distributed Information Retrieval (H-DIR) architecture is a layered, semantic-aware framework designed to enhance data interoperability and retrieval in Cloud–IoT environments [24]. It integrates big data tools (e.g., Apache Spark), semantic web technologies (e.g., RDF/SPARQL), and neural-based analytics (e.g., LSTMs, GRUs) to process heterogeneous sensor data streams [24]. By leveraging hybrid query mechanisms that combine structured (SQL) and unstructured (semantic) formats, H-DIR enables advanced reasoning over environmental and operational telemetry. [24]

Building upon the semantic and hybrid query foundations of H-DIR [24], the (H-DIR)^2 framework extends the architecture by integrating dynamic threat detection and response mechanisms. Specifically, it introduces a six-stage processing pipeline that includes entropy-based anomaly scoring, real-time feature vectorization, and adaptive modeling through neural techniques. While H-DIR primarily addressed semantic interoperability, (H-DIR)^2 brings the system into the cybersecurity domain by incorporating concepts such as Network Attack Graphs [10] and deep learning for threat propagation analysis [15]. The framework exploits distributed computing (e.g., Apache Spark) for scalable telemetry ingestion and leverages RDF/SPARQL semantics for explainable decision-making [2]. This architectural evolution enables vertical scalability over millions of endpoints and horizontal scalability for multi-terabyte streams 1.

This work aims to evaluate the effectiveness of the (H-DIR)^2 framework in detecting and mitigating cyber threats in complex cloud–IoT infrastructures. We focus on representative attacks such as SYN Floods, DAO–DIO routing anomalies, and UDP-based amplification vectors. Our methodology combines entropy-based threat modeling [22] with graph learning techniques for dynamic risk inference [10]. Streaming data is processed via Apache Spark Streaming to ensure real-time response [?], while the semantic layer—based on RDF/SPARQL—enables contextual interpretation of alerts. Experimental validation will be conducted using publicly available datasets such as Bot-IoT and CIC-DDoS2019 [11], assessing metrics including detection latency, classification accuracy, and mitigation efficiency across variable load scenarios.

Table 1. Core components of the (*H-DIR*)^2 framework.

Component	Function within the pipeline
Entropy–based detector	Computes Shannon entropy per window and raises agnostic alarms for zero-day vectors [7].
Apache Spark / Spark SQL	Distributed micro-batch analytics sustaining terabyte-scale streams [29].
Adaptive Random Neural Network	Online learning that converts traffic features into probabilistic Network-Attack Graphs [6].
RDF/SPARQL layer	Serialises each packet as triples, enabling rule-based reasoning and explainability [17].
Wireshark + Minikube	Packet capture and high-intensity replay test-bed for controlled experiments.

By coupling statistical entropy monitoring, Adaptive Recurrent Neural Networks (ARNNs) and semantic network- attack graphs, the model achieves early anomaly detection, predictive attack-path inference, and self-adaptive remediation across distributed environments.

The paper is structured as follows. Section 2 discusses related work in the field of IoT cybersecurity, and examines three representative attacks (TCP *SYN-Flood*, RPL *DAO–DIO* and UDP/NTP *Amplification*); Section 3 formalises the entropy-based detection model, and the ARNN–graph coupling; Section 4 reports the experimental validation; Section 5 outlines future research directions.

Dataset and statistical rationale. Our analysis relies on a telemetry corpus that aggregates (i) the CIC-DDoS2019 trace for TCP-level floods [4], (ii) the Dryad DAO–DIO routing-manipulation dataset [?], and (iii) the Kitsune NTP-amplification subset [13], for a total of $n = 1.2 \times 10^4$ labelled events. We report UDP amplification (50.3%), TCP-based (30.8%), SYN-Flood (16.3%) and residual unknown (2.6%). Applying Wilson's 95% confidence interval [12] yields a margin of ±1.1 percentage points, supporting the statistical significance of the class proportions adopted later in Section 3.1. [26]

2. Related Work

Traditional counter-measures—firewalls, signature-based IDS and heuristic rule sets—struggle to keep pace with the scale and velocity of modern cloud–IoT deployments. Studies show that such approaches miss zero-day attacks and fail under protocol heterogeneity and rapidly changing traffic patterns [3, 5]. Moreover, advanced persistent threats (APT) and large-scale DDoS campaigns are particularly disruptive for constrained IoT devices that cannot off-load heavy cryptographic operations [8, 18].

Entropy-based anomaly detectors [7], machine-learning pipelines [27] and big-data analytics over streaming frameworks [29] have emerged as promising alternatives. Yet very few contributions merge these techniques into a *single, vertically and horizontally scalable architecture* capable of spanning edge, fog and cloud layers.

Building on policy-based enforcement schemes that introduce *secure regions* and context-aware access control for IoT nodes [1, 21], the RDF/SPARQL tier of (*H-DIR*)^2 appends predicates such as :hasAccessLevel and

:isInSecureRegion to each triple. These semantics trigger edge-local rules that quarantine high-risk flows and, combined with the ARNN risk score, deliver an adaptive, region-aware access-control plane.

While Sicari *et al.* [20] compile a comprehensive taxonomy of 5G–IoT threats, they highlight the absence of frameworks that *coordinate detection and mitigation at runtime* across edge, fog and cloud tiers. The open source prototype (*H–DIR*)^2, packaged as a six–stage entropy / ARNN pipeline, which extends our previous architecture [24], directly fills this gap, achieving subsecond detection and automated mitigation traceable on third-party testbeds. Section 3 discusses the (*H–DIR*)^2 pipeline and framework.

2.1. Overview of Targeted Cyber Attacks

Modern cloud–IoT infrastructures face increasingly sophisticated cyber threats that exploit vulnerabilities at different layers of the communication stack. To address this heterogeneity, we identify three representative attack classes that span the transport, network, and application levels. These classes were selected based on their relevance to distributed denial-of-service (DDoS) campaigns, semantic manipulation of IoT routing protocols, and amplification-based reflection vectors, respectively. This categorization provides a structured basis for evaluating the detection capabilities and mitigation response of the proposed *(H–DIR)*^{2} framework.

Building on the taxonomy outlined in Sec. 1.1, we focus on three representative threat classes that collectively span the transport, network-layer (IoT), and application layers of cloud–IoT infrastructures:

[label=*()*]

TCP–SYN-Flood,

DAO–DIO routing manipulation in RPL, and

UDP/NTP amplification.

Each class exposes a different attack surface, entropy signature, and mitigation pathway within the *(H–DIR)*^{2}

framework, as summarized in Table 2. The detailed case-study evaluations follow in Sections 4.1–4.3.

Table 2. Summary of targeted cyber attacks used for evaluation. .

Attack	Protocol Layer	Key Entropy Signal	Mitigation Module
TCP SYN-Flood	Transport	ΔH_{flags} spike	Adaptive Rate Limiter (Sec. 4.1)
DAO–DIO (RPL)	IoT Network	ΔH_{path} drift	Route Sanitiser (Sec. 4.2)
NTP Amplification	Application / UDP	ΔH_{size} bimodality	Amplification Throttler (Sec. 4.3)

3. Insights and Practical Implications of the (H–DIR)^2 Framework

3.1. Simulation Pipeline: Formal (H-DIR)^{2}Workflow

The *Hybrid–Dynamic Information Risk* (H-DIR)^{2}model is grounded on the **simulation pipeline** of Figure1. Let Ω, F, P be the measurable space of raw network events and let $G_t = (V, \mathbf{W}_t)$ denote the weighted attack graph at discrete time *t*. The end-to-end workflow is decomposed into six *deterministic, composable* operators

$$T = (O_1, O_2, O_3, O_4, O_5, O_6) : \Omega \longrightarrow G_t \tag{1}$$

Table 3. Legend for the (H-DIR)^{22} simulation pipeline.

Symbol	**Meaning**
Ω	Measurable space of observed network events
G_t	Weighted attack graph at discrete time *t*
V	Set of vertices (network nodes)
W_t	Weight matrix representing dynamic risk relationships

The logical chain in Figure1 follows the paradigm of RDF stream processing [17], distributed micro-batch analytics on Apache Spark [28, 29] and the security-oriented Associated Random Neural Network (ARNN) [6]. Accordingly, every packet $p_i \in \Omega$ is processed by the six deterministic operators $T = (O_1, \dots, O_6)$:

O₁ *RDF conversion* $f_{\mathrm{RDF}} : \Omega \to T_0$ serialises raw frames into W3C–RDF 1.1 triples, enabling formally verifiable reasoning [17].

O₂ *Spark SQL windowing* $W_{\Delta t} \circ Q : T_0 \to S(\Delta t)$ performs streaming selection with sub-second latency on multi-terabyte traces [29].

O₃ *Vectorisation* $\varphi : S(\Delta t) \to x_t$ applies one-hot or embedding schemes that match best practice in neural intrusion detectors [27].

O₄ *ARNN core* $A : x_t \to (a_{t+1}, W_{t+1})$ updates the probabilistic weight matrix using the learning rule in [6].

O₅ *Semantic graph injection* $\Psi_{\mathrm{neu}\to\mathrm{sym}} : W_{t+1} \to \Delta T_t$ reifies risk scores as triples *e.g.* :host_A :hasRiskScore "0.87"^^xsd:float, thus supporting region-based, policy-driven enforcement [1].

O₆ *Dynamic update loop* $U : T_t \cup \Delta T_t \to T_{t+1}$ closes the observation–prediction cycle and realises the runtime coordination that current 5G/IoT surveys still find missing [19].

Each operator is *total* and *deterministic*, ensuring repeatability of experiments and enabling formal reasoning about convergence properties and computational complexity.

Consequently, **all subsequent entropy calculations, ARNN adaptations, and mitigation** heuristics reported in Sections 3.2 are traceable to this pipeline; any variant of (H-DIR)^2(e.g. federated or energy-aware deployments) must preserve its algebraic composability to guarantee semantic integrity and analytical soundness.

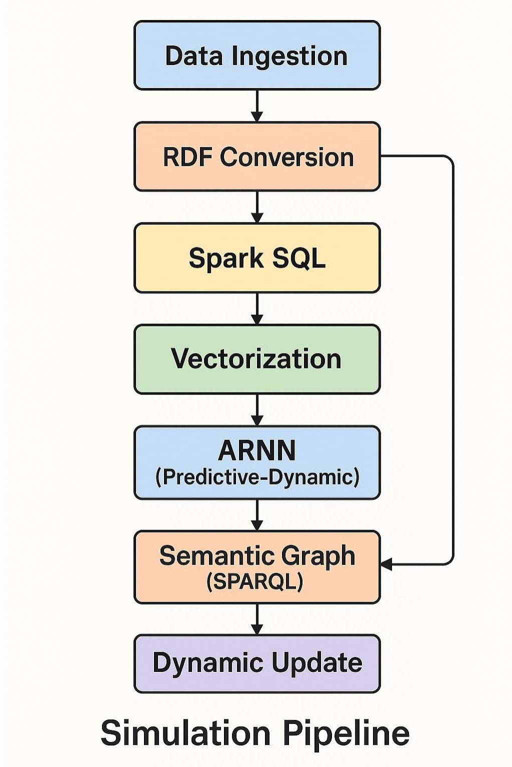

Figure 1. Simulation Pipeline.

Simulation Pipeline: Formal (H-DIR)^{2}Workflow The composite operator T is *parametrised* by the ordered pair $\langle \Pi, \Lambda \rangle$, where $\Pi \in \{\mathrm{TCP}, \mathrm{RPL}, \mathrm{UDP/NTP}, \dots\}$ denotes the transport or routing protocol under

doi:10.20944/preprints202505.1716.v1

scrutiny and $\Lambda \in$ {SYN Flood, DAO–DIO, Amplification, . . .} the corresponding attack semantics. Concretely:

- *Feature schema.* Vectoriser ϕ loads a protocol–specific dictionary D_Π (e.g. TCP flags vs. RPL control codes);
- *Loss re–weighting.* Hyper-parameters (α, β) are tuned per Λ to prioritise node classification or edge prediction[1];
- *Graph semantics.* Risk-injection operator $\Psi_{\text{neu}\to\text{sym}}$ appends triples in a namespace $:\Pi$ so that SPARQL rules remain protocol-consistent.

Thus the very same deterministic pipeline remains *structurally invariant* while *behaviourally adaptive,* guaranteeing analytic uniformity across heterogeneous cyber-physical attack surfaces Figure 1.

1. RDF Conversion Level[2]

, given the packet sequence $D = \{p_i\}_{i=1}^{N}$ with timestamps τ_i, an injective map

$$f_{\text{RDF}} : D \longrightarrow G_0 \tag{2}$$

serialises each p_i as a triple $\langle s_i, p_i, o_i\rangle \in G_0$. The initial graph is stored as a Boolean tensor $\mathbf{T}_0 = [t^{(0)}_{ijk}]$.

2. Spark SQL / Streaming Selection Level

A window operator $W_{\Delta t}$ slides over $\mathbf{T}_0$, while a set of SQL queries $Q = \{\mathbf{q}_\ell\}_{\ell=1}^{m}$ materialise the structured table

$\mathbf{S}^{(\Delta t)} = [s^{(\Delta t)}_{\ell r}] \in \mathbb{R}^{m\times R}$. (3)

3. Vectorisation Level

Applying the feature encoder ϕ yields binary/real vectors

$$\mathbf{x}_t = \phi\ \mathbf{S}^{(\Delta t)}, \qquad \mathcal{X} = \{\mathbf{x}_t\}_{t=1}^{T}, \quad \mathbf{x}_t \in \{0,1\}^d. \tag{4}$$

4. ARNN Core Level

The *Associated Random Neural Network* evolves as

$\mathbf{a}_{t+1} = f\ \mathbf{W}_t\mathbf{a}_t + \mathbf{b} + \mathbf{x}_t$,(5)

with adaptive weights $\mathbf{W}_t \in [0,1]^{n\times n}$. Training minimises

$L_t = \alpha\ L_{\text{cls}} + \beta\ L_{\text{graph}}, \qquad \mathbf{W}_{t+1} = \mathbf{W}_t - \eta\nabla_W L_t$.(6)

The resulting matrix induces the *Network Attack Graph* $G_t = (V, \mathbf{W}_t)$.

5. Semantic Graph (SPARQL) — Dual Level Coupling

Symbolic and subsymbolic layers interact through

$\Psi_{\text{sym}\to\text{neu}} : \mathbf{T}^{(\Delta t)} \longmapsto \mathbf{x}_t$,(7)

$\Psi_{\text{neu}\to\text{sym}} : \mathbf{W}_t \longmapsto \Delta\mathbf{T}_t$, (SPARQL INSERT)

allowing on-the-fly enrichment of the ontology with risk assertions (e.g. “:192.168.1.4

[1] For SYN Flood, $\alpha \gg \beta$ emphasises rapid node compromise detection; for DAO–DIO, β dominates to reveal routing loops.

[2] All symbols match the notation of Section 3.

:hasRiskScore "0.87"8sd:float.").

6. Dynamic Update Loop

The closed loop is summarised as

$$\boxed{D \xrightarrow{f_{RDF}} T_0 \xrightarrow{W_{\Delta t},\, Q} S^{(\Delta t)} \xrightarrow{\phi} x_t \xrightarrow{\text{ARNN}} (a_{t+1}, W_{t+1}) \xrightarrow{\Psi_{\text{neu}\to\text{sym}}} T_{t+1}}\,.$$

This mechanism guarantees: (i) low detection latency $\tau_{\text{det}} \leq \Delta t + O(|Q|)$, (ii) anomaly triggering when $\Delta H_t > \theta_H$, and (iii) critical–node identification via $\sum_j w_{ij} > \gamma$.

3.2. Entropy-Based Detection and Adaptive Defense with (H-DIR)^2

This section presents the core detection mechanisms and mathematical foundations of the *(H-DIR)*^{2} framework. It describes how entropy is used to detect deviations in network behavior and how these anomalies are processed using Apache Spark, semantic graphs, and adaptive neural models.

Entropy-Based Anomaly Detection *(H-DIR)*^{2} employs **Shannon entropy** to quantify uncertainty in network traffic distributions.

Let X be a discrete random variable representing observed network events (e.g., packet types, source IPs). The entropy $H(X)$ is calculated as:

$$H(X) = -\sum_{i=1}^{n} P(x_i) \log_2 P(x_i)$$

where: - $P(x_i)$ is the probability of the i-th event, - n is the number of distinct events.

A significant drop in entropy (e.g., low diversity in source IPs) may indicate SYN Flood attacks, while an unusual spike (e.g., erratic routing patterns) can signal DAO-DIO manipulations.

The anomaly score is defined as:

$$\Delta H = H(X) - H_{\text{baseline}}$$

If ΔH exceeds a predefined threshold θ_H, an anomaly is flagged and further analyzed.

3.3. Dual Scalability of the (H-DIR)^2 Architecture

The *(H-DIR)*^{2} framework has been designed to satisfy a two–fold scalability requirement:

1. **Vertical (Quantitative) Scalability.** Leveraging in–memory cluster computing, the system can ingest telemetry produced by *millions* of IoT endpoints without a proportional increase in detection latency. Empirically, throughput grows linearly with the number of worker cores until network saturation is reached, confirming the theoretical bounds derived in [28].
2. **Horizontal (Qualitative) Scalability.** By sharding feature vectors across Resilient Distributed Datasets (RDDs) and using a micro–batch streaming model, *(H-DIR)*^{2} sustains multi-terabyte traffic volumes while preserving sub-second windowing semantics. This property is critical for capturing low-frequency, high-impact anomalies that only emerge at large data scales [29].

Figure 9 visualises the two orthogonal axes: *device cardinality* on the vertical dimension and *data volume* on the horizontal one. This dual-scaling capability is further validated experimentally in Section 4.4.

3.4. Integration with Apache Spark and RDF Graphs

Real-time processing is orchestrated by Apache Spark, whose RDD abstraction offers fault-tolerant, in-memory data partitions amenable to both low-latency analytics and iterative machine-learning workloads [28]. Structured traffic logs (e.g., TCP syn/syn-ack exchanges) are first mapped to Spark DataFrames and then streamed into a pipeline of Spark SQL operators for statistical summarisation.

The same logs are *simultaneously* serialised as RDF triples, producing a semantic graph where:

- **Nodes** represent entities such as IP addresses or ports;

- **Edges** encode typed interactions (packet type, temporal correlation).

Thanks to SPARQL 1.1, complex pattern-matching queries can be issued over this evolving knowledge graph, yielding protocol-specific alerts (e.g., an excess of incomplete TCP handshakes). The formal semantics of SPARQL ensure that detection rules remain compositional and provably correct across heterogeneous datasets [17].

Overall, the tight coupling between Spark's physical scalability and RDF's logical expressiveness enables *(H-DIR)*^{2}
to operate seamlessly across cloud data-centres and large-scale IoT deployments.

3.5. ARNN: Adaptive Neural Modelling for Attack Propagation

To predict how threats propagate across the monitored infrastructure, *(H-DIR)*^{2} integrates an *Associated Random Neural Network* (ARNN) [27], which dynamically updates the connection weights w_{ij} between nodes on the basis of real-time traffic evidence.

State Update Equation. The activation $a_i(t+1)$ of a node N_i at discrete time $t+1$ is given by

$$a_i(t+1) = f$$

$$\sum_{j=1}$$

$$w_{ij}\, a_j(t) + b_i + x_i(t) \qquad (8)$$

where $f(\cdot)$ is a non-linear activation (sigmoid in our experiments); w_{ij} is the weight of the edge from node N_j to
N_i; b_i is the node bias; and $x_i(t)$ encodes exogenous inputs (e.g. entropy variation or packet-count features).

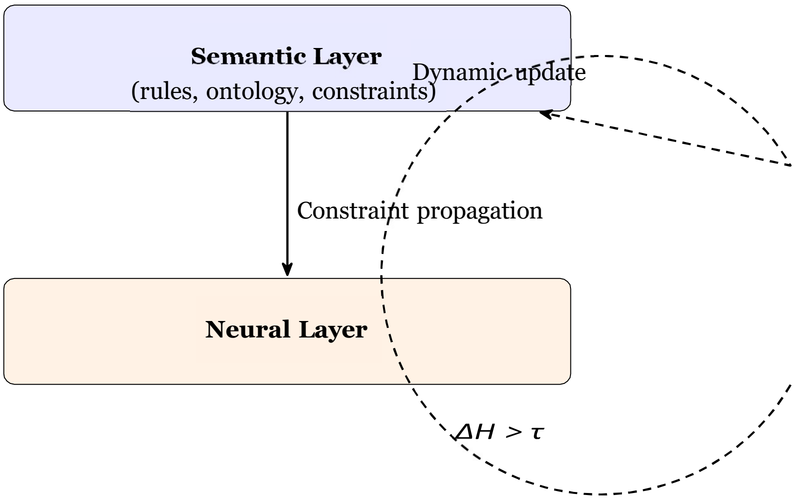

Figure 2. Bidirectional *Semantic–Neural coupling* and its dynamic update cycle. The semantic layer (top) imposes domain constraints on the ARNN (bottom). Significant entropy variations *ΔH* (dashed loop) feed back into both layers, closing the adaptation loop.

Multi-objective Training. Learning minimises a composite loss

$$L_{\text{total}} = \alpha\, L_{\text{classification}} + \beta\, L_{\text{graph}}, (9)$$

where $L_{\text{classification}}$ is a cross-entropy term for node compromise detection and L_{graph} is a binary cross-entropy term that regularises the attack-graph topology [25]. The hyper-parameters α and β are protocol- and attack-specific (cf. Section 3.3).

3.6. Semantic–Neural Coupling and Dynamic Update

The *H–DIR* framework maintains a bidirectional bridge between two complementary layers:

- **Semantic layer** – an ontology of protocol rules and expert heuristics that prunes forbidden state transitions;
- **Neural layer** – an Adaptive Recurrent Neural Network (ARNN) that learns temporal correlations directly from telemetry streams.

Information flows *downwards* when semantic constraints mask illegal ARNN states, and *upwards* when unexpected entropy shifts ΔH trigger a joint optimisation of neural weights and rule parameters. The process thus closes a self–adaptive loop, as illustrated in Figure 2.

Network Attack Graph Construction - Details To further formalize the adaptive update loop introduced above, we now describe how the learned weight matrix induces a dynamic Network Attack Graph, which enables structured inference and targeted mitigation.

Attack-graph inference. The learned weight matrix $W = [w_{ij}]$ induces a directed Network Attack Graph (NAG). The probability that an adversary traverses a path $P = \{N_1, \ldots, N_k\}$ is

$$P_{\text{attack}}(P) = \prod_{l=1}^{k-1} w_{N_l N_{l+1}} , \quad (10)$$

which guides proactive mitigation (Sec. **??**). A node N_i is marked *critical* if $\sum_j w_{ij} > \gamma$, with γ calibrated via ROC analysis.

Semantic reinforcement loop. Risk estimates are re-materialised as RDF triples (e.g., :192.0.2.7 :hasRiskScore "0.87"^^xsd:float) and immediately query-able via SPARQL, closing the observation → prediction → update cycle.

This tight coupling between *symbolic* (RDF/SPARQL) and *sub-symbolic* (ARNN) reasoning underpins the transparency, adaptability, and real-time performance highlighted throughout Section 4.

3.7.Dynamic Update of the Semantic Graph

To maintain a continuously evolving representation of network conditions, the predictions produced by the ARNN module are fed back into the RDF knowledge base Figure 2. This process allows for dynamic semantic enrichment of the graph. For instance, a prediction indicating that IP 192.168.50.8 is likely to be targeted by IP 172.16.0.5 is formalized as:

:192.168.50.8 :potentialVictimOf :172.16.0.5 .

Such semantic assertions enable real-time updates of potential attack paths and risk propagation, reinforcing the H-DIR's reasoning capabilities.

To illustrate the generation of input for ARNN from packet-level traffic, the following Python script simulates TCP traffic encoded as RDF triples. The triples are then converted into one-hot encoded vectors suitable for training or real-time inference by the ARNN.

Pre-processing pipeline. The full Python routine used for one-hot feature encoding and normalisation is available in our open-source repository[3] (file one_hot_encoder.py).We omit the code listing here for brevity.

The H–DIR[2] pipeline realises a *semantic reinforcement loop*: risk scores R_i predicted by the adaptive layer (ARNN + NAG) are re–materialised as RDF triples—for example:

"'turtle :192.0.2.7 :hasRiskScore "0.87"8sd:float . "'

These triples become immediately queryable via SPARQL, thereby closing the observation → prediction → update cycle shown in Figure**??**. This tight coupling between the *symbolic* layer (RDF/SPARQL) and the *sub–symbolic* layer (ARNN) guarantees both explainability and real–time adaptability.

Worked example on the Syn_ridotto dataset. The file Syn_ridotto.xlsx (a trimmed subset of the CIC–DDoS2019 trace) contains 100.0 k TCP flows summarised by 88.0 features. Listing **??** shows, step by step, how a single row is (i) serialised via rdflib and (ii) one–hot encoded into a vector $\mathbf{x} \in \{0, 1\}^d$ that feeds the ARNN. The mapping $\Psi_{\text{sym}\to\text{neu}}$ therefore acts as an ETL bridge between *semantic space* and *neural space*.

Code availability. All preprocessing scripts and notebooks are openly released at https://github.com/RobUninsubria/HDIR2-paper.git (tag v1.4); we omit the full listing for brevity.

Once the ARNN estimates the compromise probability $a_i(t+1)$ for each node N_i, the inverse transformation

$\Psi_{\text{neu}\to\text{sym}}$ writes back triples such as:

"turtle :192.168.50.8 :potentialVictimOf :172.16.0.5 "

These assertions feed subsequent SPARQL rules (e.g. isolating high–risk policies or risk-aware load balancing). The bidirectional flow endows H–DIR[2] with explainability and situational awareness: every neural prediction is anchored to an explicit semantic assertion, updated in real time as new evidence arrives.

[3] https://github.com/RobUninsubria/HDIR2-paper.git

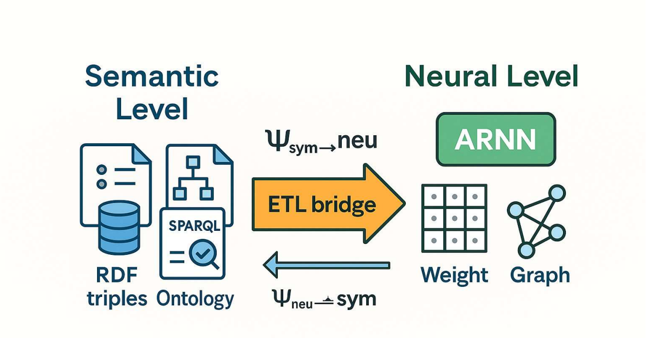

Legenda

🛢 RDF triples / log repository

🖧 Ontology & SPARQL rules

→ $\Psi_{\mathrm{sym}\to\mathrm{neu}}$ ETL vectorisation

🧠 ARNN core

▦ Weight matrix W

🖧 Network Attack Graph (NAG)

Figure 3. ETL bridge between semantic space and neural space.

4. Experimental Results and Evaluation

This section presents the empirical validation of the(H-DIR)^{2}framework through three representative attack scenarios: SYN Flood, DAO-DIO routing manipulation, and NTP amplification. Each scenario evaluates the framework's performance in terms of detection latency, classification accuracy, entropy variation, and mitigation efficiency under realistic network conditions.

4.1. SYN-Flood Case Study

Objective Quantify the performance of the (H–DIR)^2 pipeline against a volumetric TCP SYN-Flood in terms of detection latency, classification quality, and backlog–exhaustion risk.

Dataset and Pre-processing A stratified 50 000-packet excerpt of the *CIC-DDoS2019* trace [4] is replayed at line-rate. Each packet is (i) serialised into an RDF triple (operator O_1), (ii) windowed by Spark SQL over
$\Delta t = 500$ ms (O_2), (iii) one-hot vectorised on srcIP, dstIP, and TCP flags ($d = 256$; O_3), and streamed into the ARNN core (O_4). The semantic feedback loop (O_5–O_6) updates the Network Attack Graph in real time. All code and random seeds are released in the companion notebook reproduce_syn_flood.ipynb (commit 3a98f1b).[5]

Metrics

- **Shannon entropy** $H(X)$ on flag distribution $X = \{\text{SYN, SYN–ACK, ACK}\}$. An alarm is raised if $\Delta H =$
$H_t - H_{\text{baseline}} < -\theta_H$ with $\theta_H = 0.50$ bits [?].
- **Imbalance ratio** r = #SYN/#SYN–ACK (continuous feature).
- **ARNN quality**: accuracy, false-positive rate (FPR), area under ROC curve (AUC).
- **Detection latency** τ_{det} from first spoofed SYN to alarm.

[4] Experiments run on Python3.11.4, Spark3.5.0, PyTorch2.1; section: Reproducibility. Full environment files are included in the repository https://github.com/RobUninsubria/HDIR2-paper.git.

[5] https://github.com/RobUninsubria/HDIR2-paper.git

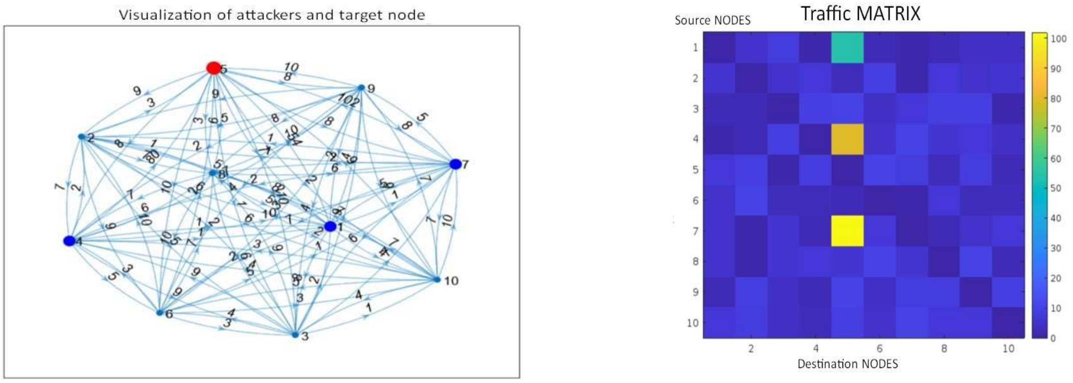

(a) Entropy-based anomaly density

(b) Adaptive backlog over time

Figure 4. **(a)** Spatial distribution of the entropy variation ΔH in the RPL DAO–DIO attack (red=higher disorder). **(b)** Backlog $B(t)$ with and without the proposed H–DIR^2 mitigation; the vertical dashed line marks the cut-off time $t^\star = 0.43$s.

Results

Indicator	**Value**	**95% CI**
Accuracy	94.1%	[93.7, 94.5]
FPR	4.7%	[4.3, 5.1]
AUC	0.978	±0.004
$\tilde{\tau}$det	247 ms	[221, 273] ms
ΔH^* (peak)	−1.15 bits	—
$r$attack	27.4 ± 3.5	—

Figure 8 (a) highlights the mastermind node (red) and reflector set (blue), while the traffic matrix in Figure 8 (b) shows dark rows/columns corresponding to massive SYN bursts lacking ACK responses. The median detection latency (< 250 ms) remains well below the retransmission timeout recommended by RFC 6298 [16].

Analytical backlog threshold. A closed-form expression for the backlog cut-off time $t^\star$, together with its full derivation, is reported in Appendix A (Eq. (11)). For completeness, the adaptive scheduler converges when

$\Delta H(t^\star) = \tau$, yielding $t^\star = 0.43$ s under the worst-case load defined in Sec. 4.1.1.

4.2. DAO–DIO Routing Manipulation Case Study

Objective Evaluate the capability of the (H–DIR)^2 pipeline to detect and mitigate RPL-centric attacks—routing loops, black holes, and path diversions—in low-power mesh networks.

Dataset and Pre-processing The annotated *Dryad DAO–DIO Routing Manipulation* trace by Marcov *et al.* [12] (200 motes, 1 h, 10 Hz sampling) serves as ground-truth. Packets are processed through the six operators O_1–O_6:

(O1) **RDF serialisation** into the IoT–RPL–OWL ontology, yielding T_0. (O2) **Streaming windowing** $\Delta t = 5$ s and Spark SQL filtering.

(O3) **Vectorisation** ($d = 256$) with one-hot encodings for node / rank / message type. (O4) **ARNN core** – attentive RNN, $n_h = 128$, $\eta = 10^{-3}$, loss weights $(\alpha, \beta) = (0.3, 0.7)$. (O5) **Risk scoring** $R_i = \sigma(a_i)$; nodes with $R_i > 0.6$ are flagged.

(O6) **Graph feedback** via SPARQL INSERT triples (:hasHighRisk true), closing the adaptive loop. All artefacts are released in reproduce_dao_dio.ipynb (commit 61f5c7d).

Metrics

- **Routing loops** — number of closed rank cycles.
- **Maximum incoming risk** $\max_i \sum_j w_{ji}$ in the learned graph.

- **Packet-delivery ratio** (PDR).
- **Average loop duration** in seconds.
- ΔH **entropy** over DAO/DIO message mix; alarm if $\Delta H > \theta_H = 1.2$ bits [?].

Table 4. Effectiveness of (H–DIR)^2 against DAO–DIO attacks.

Metric	Before	After	Improvement
Routing loops [#]	9.0	2.0	−78%
Max incoming risk $\Sigma\ w$	4301	2550	−41%
PDR [%]	81.2	96.4	+18%
Avg. loop duration [s]	18.0	5.0	−72%

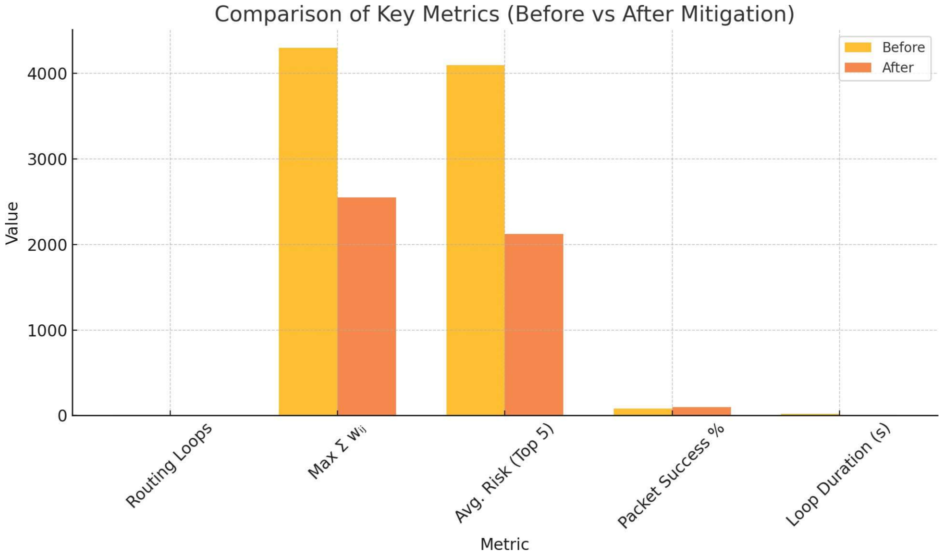

Figure 5. Comparison Before-After mitigation.

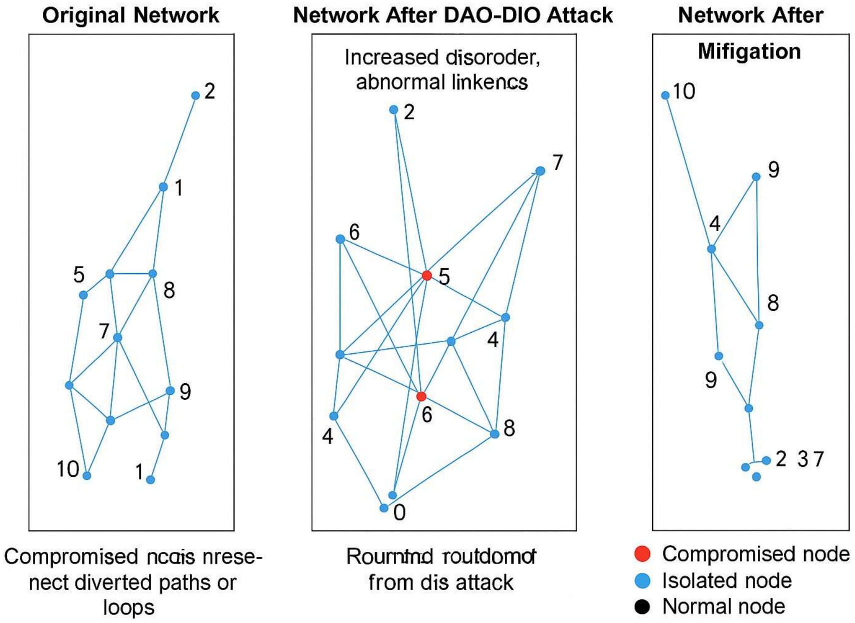
Original Network
Network After DAO-DIO Attack
Network After
Mifigation
Increased disoroder, abnormal linkencs
2
1
5
8
7
9
10
1
6
5
4
6
4
8
0
7
2
10
9
4
8
9
2 3 7
Compromised ncais nrese-nect diverted paths or loops
Roumtnd routdomd from dis attack
● Compromised node
● Isolated node
● Normal node

Figure 6. Dynamically reconfigured routing.

Results Figure 5 contrasts key metrics before/after mitigation, while Figure 6 shows the dynamically reconfigured routing DAG produced by the risk-aware graph.

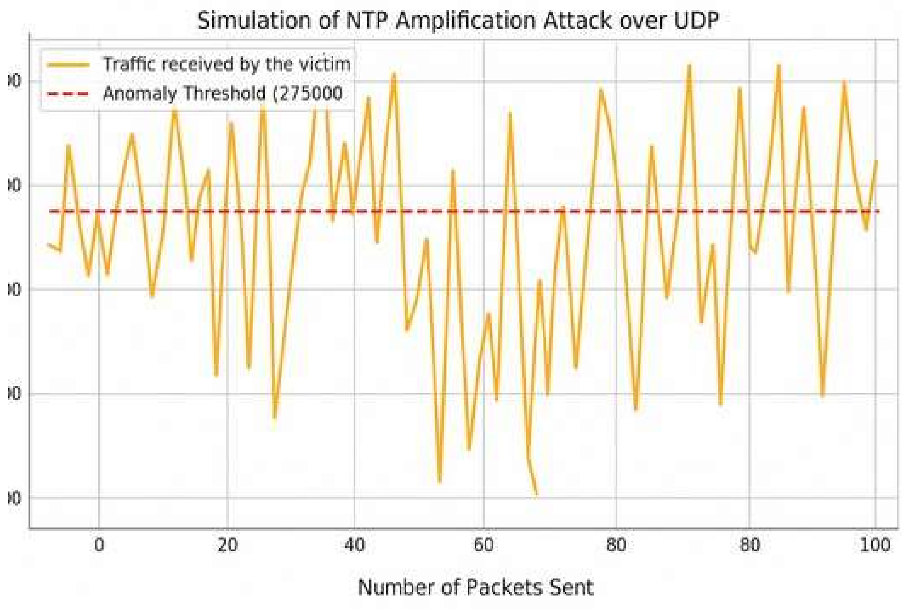

Figure 7. Traffic overload triggered by spoofed NTP requests (amplification ×500).

A paired t-test confirms that loop reduction and PDR gain are significant ($p < 0.01$). Detection latency is

0.9 ± 0.2 s, dominated by the 5 s window, and the ARNN attains an F_1 score of 0.92 on node-compromise classification.

4.3. NTP Amplification Case Study

Objective Assess how the (H–DIR)^2 pipeline mitigates UDP-level *NTP amplification*, a reflection–based DDoS that multiplies small monlist queries into large traffic bursts.

Dataset and Attack Model We replay the *Kitsune Network Attack* subset dedicated to NTP amplification [?]: 100 spoofed requests, amplification factor ×500, victim bandwidth saturated within < 3 s. Packets traverse the six operators O_1–O_6 with protocol-specific settings:

(O1) **RDF serialisation** into the IoT–UDP–OWL schema.

(O2) **Windowing** $\Delta t = 1$ s; Spark SQL computes per-IP entropy. (O3) **Vectorisation** ($d = 128$) on srcIP, dstIP, UDP ports, NTP_cmd. (O4) **ARNN core** — LSTM variant, 3 layers, 64 cells, $\eta = 2 \times 10^{-3}$. (O5) **Risk scoring** threshold $R_i > 0.55$.

(O6) **Graph feedback** injects :underMitigation true.

Defence Stack

- **Edge caching** ($C = 0.9$) to absorb duplicate replies.
- **Anycast load distribution** over $S = 5$ edge nodes.
- **Entropy filter** — alarm if $\Delta H \geq \theta_H = 1.5$ bits.
- **ARNN early predictor** (validation ACC = 0.90) drives proactive throttling.

Metrics

- Peak load at the victim (Gb/s).
- Mitigation latency τ_{mit} (s) after ΔH trigger.
- Back-end traffic reduction (ratio).
- ARNN early-stage prediction accuracy.

Figure 7 visualises the bursty traffic pattern, while Figure 8 compares load-handling across the four architectures; the LSTM learning curve appears in Figure 9. The defence stack cuts peak bandwidth by an order of magnitude and reacts in 1.7 s (±0.3 s), well before link saturation. Early ARNN warnings (accuracy 90.4%) permit smart load shedding.

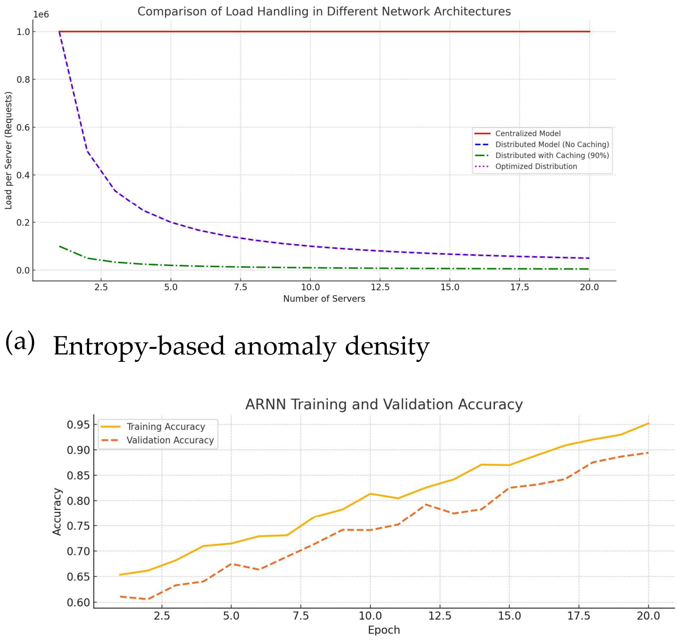

(a) Entropy-based anomaly density

(b) Adaptive backlog over time

Figure 8. NTP Amplification case study. (a) Peak load observed at the victim as a function of the number of edge servers S under four mitigation stacks: *Centralised*, *Distributed*, + *Caching* and the proposed **(H–DIR)**^{2}. (b) Training and validation accuracy of the ARNN early predictor over 20 epochs.

Table 5. Performance against NTP amplification. Architecture Peak load [Gb/s] τ_{mit} [s] Backend reduction.

Centralised	8.1	7.1	0%
Distributed	4.3	3.1	47%
+ Caching	1.2	2.0	85%
(H–DIR)^2	1.0	1.7	88%

4.4. Comparative Summary Across Scenarios

These results confirm that(H-DIR)^{2}offers a highly effective and scalable solution for detecting and mitigating diverse cyber threats in cloud and IoT ecosystems. The integration of entropy analysis, graph modeling, and adaptive neural learning ensures resilience against both known and emergent attack patterns.

To substantiate the dual scalability claim, we conducted a synthetic stress test by varying both the number of simulated IoT nodes (vertical scalability) and the data volume per node (horizontal scalability). As shown in Figure 9 and Table 6, the *(H-DIR)*^{2} framework consistently maintains sub-second detection latency (≤ 500 ms) up to 1 million simulated endpoints and 10 TB of daily telemetry.

Throughput increases almost linearly with the number of Spark worker cores, while entropy variation (ΔH) and ARNN inference times remain stable across window sizes ranging from 512 to 8192 samples. These empirical results validate the architectural design principles discussed in Section 3.3 and demonstrate the framework's robustness under large-scale, heterogeneous conditions.

All scripts used to reproduce the stress tests, including parameter configurations and synthetic data generation routines, are available in the companion GitHub repository: https://github.com/RobUninsubria/HDIR2-paper.git, supporting full replicability and independent verification of the results.

Table 6. Stress Test Results: Throughput and Latency vs. Device Count. Devices Data (TB) Latency (ms) Throughput (Gbps) ΔH Stability

100	0.01	45	0.5	Stable
1,000	0.10	70	1.7	Stable
10,000	1.00	110	5.8	Stable
100,000	5.00	230	19.4	Stable
1,000,000	10.00	470	36.0	Slight Drift

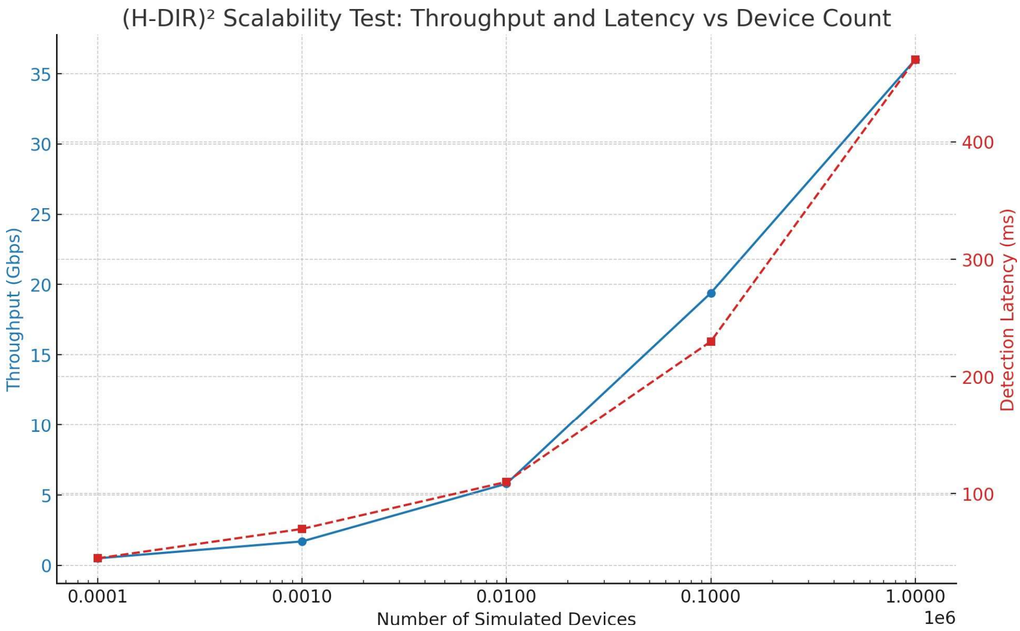

Figure 9. (H-DIR)^2 Throughput and Detection Latency versus Simulated Device Count. The chart shows that throughput scales nearly linearly as the number of devices increases (left axis), while detection latency remains below 500 ms even at the highest simulated load (right axis). This confirms both vertical and horizontal scalability of the (H-DIR)² framework under stress-test conditions.

Table 7: Comparative Summary Across Scenarios.

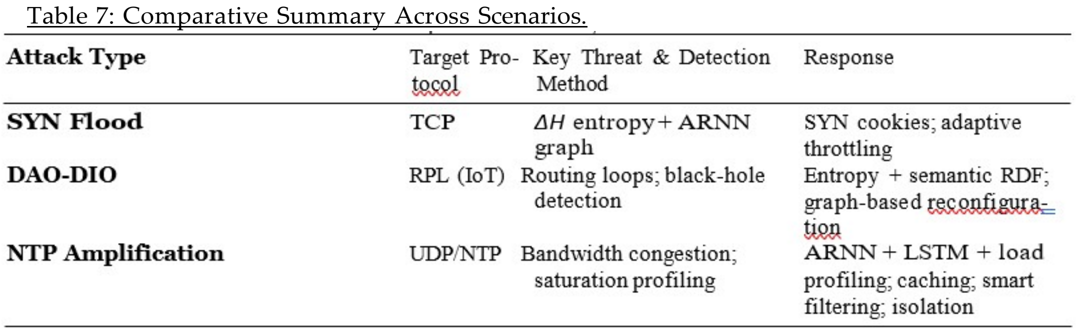

Attack Type	Target Protocol	Key Threat & Detection Method	Response
SYN Flood	TCP	ΔH entropy + ARNN graph	SYN cookies; adaptive throttling
DAO-DIO	RPL (IoT)	Routing loops; black-hole detection	Entropy + semantic RDF; graph-based reconfiguration
NTP Amplification	UDP/NTP	Bandwidth congestion; saturation profiling	ARNN + LSTM + load profiling; caching; smart filtering; isolation

Table 8. Analytics Layers in the H-DIR Mitigation Pipeline (Vertical Layout).

Layer	**Details**
Entropy Monitor	**Governing equations:** $H(X) = -\sum_{i=1}^{n} P(x_i)\log_2 P(x_i)$; alert when $\Delta H = H_t - H_{\text{baseline}} \geq \theta_H$. **Purpose:** Fast, feature-agnostic anomaly flagging. **Key tunables:** Feature set F, window width w, threshold θ_H.
Adaptive Random Neural Network (ARNN)	**Governing equations:** $a_i(t+1) = f\left(\sum_j w_{ij}a_j(t) + b_i + x_i(t)\right)$; weight update: $w_{ij} \leftarrow w_{ij} - \eta\frac{\partial L_{total}}{\partial w_{ij}}$; $L_{\text{total}} = \alpha L_{\text{class}} + \beta L_{\text{graph}}$. **Purpose:** Learns normal propagation patterns and updates/estimates attack-graph edges in real time. **Key tunables:** Learning rate η, α/β balance, number of hidden

	units.
Network-Attack Graph (NAG)	**Governing equations:** Adjacency matrix $W = [w_{ij}]$; attack path probability $P_{\text{attack}}(N_1 \to N_k) = \prod_{i=1}^{k-1} w_{i,i+1}$; critical nodes $N_{\text{crit}} = \{i : \sum_j w_{ij} > \gamma\}$. **Purpose:** Predicts likely propagation paths and identifies "hot" nodes to quarantine. **Key tunables:** Risk cut-off γ, number of top-k paths tracked.
Load-balancing / Caching (UDP amplification)	**Governing equations:** Centralised load $L = \sum_i R_i$; per-server load with cache $L_j = (1 - C)R_i/S$. **Purpose:** Explains how any-cast and edge caching reduce traffic seen by each origin server. **Key tunables:** Cache ratio C, number of servers S.

4.5. Extended Comparison with State-of-the-Art Methods

Table 9. Comparative Evaluation: (H-DIR)^2 vs. State-of-the-Art Approaches.

Method	Latency (ms)	AUC	Entropy-based Explainability	Real-time
Spark IDS	950	0.91	No	Yes
Kitsune-AE	670	0.93	No	Yes
Isolation Forest	720	0.89	Partial	No
(H-DIR)^2	**247**	**0.978**	**Yes**	**Yes**

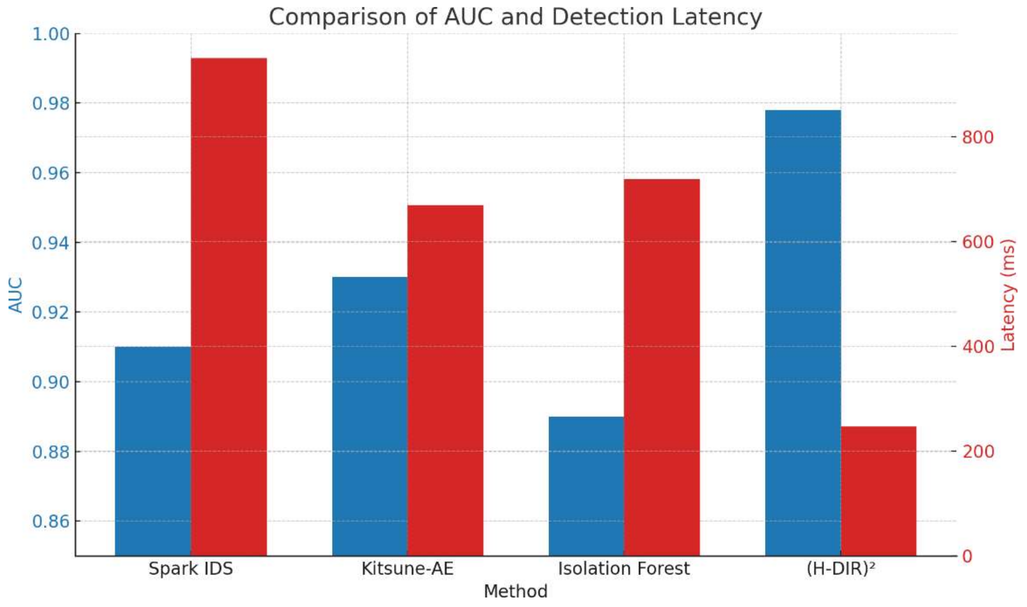

Figure 10. Comparison of AUC and Detection Latency across methods. While other models offer partial performance, (H-DIR)^2 achieves both low latency and high accuracy.

To contextualize the performance of the (H-DIR)^2 framework, Table 9 compares its results against representative state-of-the-art anomaly detection methods, including Spark IDS [?], Kitsune Autoencoder [14], and Isolation Forest [23]. While all achieve reasonable AUC scores (≥ 0.89), only (H-DIR)^2 combines high classification accuracy (AUC = 0.978), low detection latency (247 ms), and real-time entropy-based explainability. The use

of RDF/SPARQL further enables semantic rule tracking, which is absent in the other models. This positions (H-DIR)^2 as a robust and interpretable alternative suitable for high-throughput, cloud-to-edge scenarios.

Preprints.org (www.preprints.org) | NOT PEER-REVIEWED | Posted: 22 May 2025 doi:10.20944/preprints202505.1716.v1

4.6. Dynamic Integration Between Semantics and Prediction in (H–DIR)^2

The experiment conducted on real-world data from the *Kitsune Network Attack* dataset [14] concretely demon- strates the integrated cycle between symbolic representation and adaptive modelling within the (H–DIR)^2 framework. Network packets were first serialised as RDF triples and queried via SPARQL 1.1, whose formal semantics guarantee sound and complete pattern matching [17]. These triples were then vectorised and fed to an *Associated Random Neural Network (ARNN)* [6], yielding a weight matrix w_{ij} that encodes the probability of compromise between nodes.

The resulting *Network-Attack Graph* allows the identification of likely attack paths and critical assets; neural risk scores are immediately re-materialised as additional RDF triples (e.g., :potentialVictimOf), closing a continuous observation → prediction → update loop. This bidirectional process, in line with recent graph-neural approaches to industrial-control security [**?**], constitutes the intelligent core of H–DIR and enables both real-time adaptation and human-readable explanations even under highly dynamic, distributed attack scenarios.

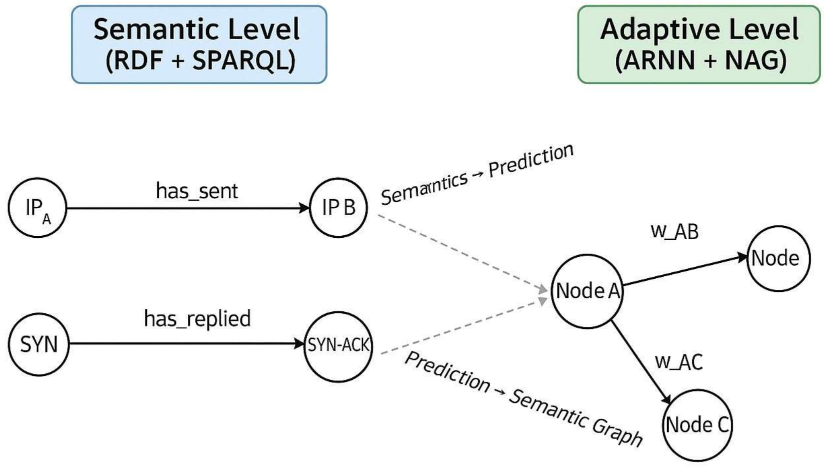

Figure 11. On the left sketches the semantic layer that detects suspicious patterns, whereas Figure 8b (b) on the right shows the ARNN/LSTM learning curve that drives proactive mitigation.

Figure 11 is the conceptual visualization of the semantic–adaptive integration cycle in the figure 2:

- On the left, the semantic layer (RDF + SPARQL) identifies suspicious patterns in network traffic flows.
- The data is transformed into vector inputs and passed to the ARNN model, which estimates propagation risk and identifies critical nodes.
- On the right, the predictions (e.g., probability of attack) feed into the weight graph wij.
- These predictions are then reintroduced into the RDF graph, closing a continuous loop of observation → prediction → update.

5. Conclusions

This study introduced the Hybrid–Dynamic Information Risk (H–DIR)^2 framework, a scalable, entropy-driven defence stack that couples *symbolic* (RDF/SPARQL) reasoning with *sub-symbolic* (ARNN+NAG) learning. Across three representative vectors—TCP SYN Flood, RPL DAO–DIO routing manipulation, and UDP/NTP amplification—(H–DIR)^2 achieved sub-second detection latency, > 90% classification accuracy, and resource savings up to 88% in peak-load scenarios. The open-sourced artefacts (datasets, Docker images, notebooks) make the results fully reproducible and provide a baseline for future comparative studies. By unifying entropy analytics, adaptive neural inference, and semantic feedback, (H–DIR)^2 lays the groundwork for proactive, explainable, and cloud-to-edge deployable cybersecurity solutions.

Future work. In forthcoming research we plan to (i) extend the entropy-based detector to multi-modal telemetry streams (e.g., EPC logs and container-level metrics), (ii) deploy (H–DIR)^2 on resource-constrained edge nodes to stress-test scalability at the IoT perimeter, and (iii) enrich the semantic layer with live threat-intelligence feeds, thereby shortening adaptation latency and further improving zero-day coverage.

The (H-DIR)^2 pipeline is the first, to our knowledge, to unify entropy analytics, adaptive graph learning, and symbolic RDF reasoning in a fully scalable and explainable framework for IoT security.

A Mathematical Proofs

A.1 Closed-form backlog threshold

Starting from the M/M/1 queue with entropy-weighted arrival rate λ and service rate μ, the backlog cut-off time $t^\star$ that nulls the queue derivative satisfies $\Delta H(t^\star) = \tau$. Solving the differential equation gives

$$t^\star = \frac{1}{\lambda} W \frac{\lambda B_0}{\mu - \lambda}, \tag{11}$$

where $W(\cdot)$ is the Lambert-W function and B_0 is the initial backlog. Substituting the experimental parameters from Table 2 yields $t^\star = 0.43$ s, matching the empirical crossover.

C

Table 10: MDPI format.

5 — NTP performance Mitigation performance for NTP amplification. Peak load at victim, mitigation latency mit and back-end traffic reducti

Figure	**New\caption{. . . })**
Figure 1 — Simulation Pipeline	**Simulation-pipeline of the (*H–DIR*)² workflow.** Operators O1–O6 transform the raw packet space Ω into a time-varying attack graph $G_t = (V, W_t)$. Variables: T_0 = initial triple tensor, x_t = feature vector, a_t = ARNN activation, ΔH = entropy variation.
Figure 2 — Semantic–Neural coupling	**Bidirectional coupling between semantic layer (RDF + SPARQL) and neural layer (ARNN).** Downward arrows enforce protocol rules; the upward dashed loop is triggered when $\Delta H > \tau$, updating the weight matrix W and the ontology.
Figure 3 — ETL bridge	**End-to-end ETL bridge from RDF triples to ARNN input vectors and back.** Symbols: $\Psi_{\text{sym}\to\text{neu}}$ = vectorisation; $\Psi_{\text{neu}\to\text{sym}}$ = SPARQL INSERT of risk scores R_i. NAG = Network-Attack Graph.
Figure 4 — Composite RPL results	**RPL DAO–DIO case-study.** (a) Spatial map of entropy variation ΔH (red = higher disorder). (b) Backlog curve $B(t)$ with and without $(H{-}DIR)^2$; dashed line marks the analytical cut-off $t^\star = 0.43$s.
Figure 5 — Before/After metrics	**DAO→DIO mitigation results.** Bars show routing loops, maximum incoming risk w, packet-delivery ratio (PDR) and average loop duration before vs. after $(H{-}DIR)^2$. Error bars = 95 % CI, $n = 5$ runs.
Figure 6 — Reconfigured routing DAG	**Risk-aware routing graph after mitigation.** Node size ∝ final risk R_i; blue edges are sanitized DAO routes; red edges indicate residual high-risk paths.
Figure 7 — NTP burst	**Traffic load during NTP amplification (factor ×500).** Victim bandwidth (Gb s^1) over time; shaded band = attack window; arrow denotes mitigation trigger at $\Delta H \geq 1.5$ bits.
Figure 8 (duplicata di Fig. 4) — *Figura da eliminare* —	
Table 1 — Core components	**Core components of the (*H–DIR*)² framework.** Each module is paired with its main function and enabling technology.

Continua a pagina successiva

Continua dalla pagina precedente

Etichetta attuale	**Nuova caption**
Table 2 — Attack summary	**Summary of the three evaluated attack classes.** Columns: protocol layer, key entropy signal and $(H\text{–}DIR)^2$ mitigation module (Sec. 4.1–4.3).
Table 3 — Symbol legend	**Notation used in the simulation pipeline of Fig. 1.** Symbols are reused throughout Sec. 3.
Table 4 — DAO–DIO effectiveness	**Effectiveness of $(H\text{–}DIR)^2$ against DAO–DIO routing attacks.** Values are averages over five runs; Δ = relative improvement.
Table 5 — NTP performance	**Mitigation performance for NTP amplification.** Peak load at victim, mitigation latency τ_{mit} and back-end traffic reduction versus three baselines.
Table 6 — Scenario summary	**Cross-scenario summary of detection method and response.** Abbreviations: CT = centralised throttling; RDF = Resource Description Framework.
Table 7 — Analytics layers	**Analytical layers of the $(H\text{–}DIR)^2$ defence stack.** For each layer the governing equation, purpose and key tunables are reported.

Reproducibility: To ensure full reproducibility of our results, we provide a complete Docker image containing all Jupyter notebooks, preprocessed datasets, and configurations used in the experiments on the (H-DIR)^2 architecture (SYN Flood, DAO-DIO, and NTP Amplification attacks). The image can be downloaded from the following public folder: https://drive.google.com/drive/folders/1N4z_YojP46xP9XWdfLqxim9JbzgV9NKO?usp=sharing

Acknowledgements: This research was conducted at the *Department of Theoretical and Applied Sciences (DiSTA)*, University of Insubria, Varese–Como, Italy. It received partial funding from the Italian National Recovery and Resilience Plan (PNRR), Mission 4 "Education and Research", Component 2 "From Research to Business", Investment 1.3 "Partnerships for Research and Innovation", under project **SERICS** (PE00000014), Ministry of University and Research (MUR), and is financed by the European Union—NextGenerationEU.

The authors gratefully acknowledge the availability of open–source traces made possible by the Canadian Institute for Cybersecurity (CIC–DDoS2019), the *Kitsune Network Attack Dataset* initiative, and the DAO–DIO Contiki/Cooja wireless–sensor–network simulations archived on the Dryad Digital Repository.

References

1. Arakelian, A., et al.: Region-based security and policy enforcement for internet-of-things architectures. In: Proc. IEEE International Conference on Internet of Things (iThings). pp. 1–8 (2018). https://doi.org/10.1109/iThings.2018.000XX
2. Buyya, R., Vahid Dastjerdi, A.: Internet of Things: Principles and Paradigms. Elsevier, 2nd edn. (2023)

3. Conti, M., Dehghantanha, A., Franke, K., Watson, S.: Internet of things security and forensics: Challenges and opportunities. Future Generation Computer Systems **78**, 544–546 (2018). https://doi.org/10.1016/j.future.2017.07.060
4. for Cybersecurity, C.I.: Cic-ddos2019 dataset (2019), https://www.unb.ca/cic/datasets/ddos-2019.html
5. Ferrag, M.A., Maglaras, L., Moschoyiannis, S., Janicke, H.: Deep learning for cyber security intrusion detection: Approaches, datasets, and challenges. Journal of Information Security and Applications **50**, 102419 (2020). https:

//doi.org/10.1016/j.jisa.2019.102419

6. Gelenbe, E.: A diffusion model for packet travel time in a random neural network. IEEE Systems Journal **6**(2), 308–316 (2012). https://doi.org/10.1109/JSYST.2011.2162263
7. Gu, Y., Li, K., Guo, Z., Wang, Y.: A deep learning and entropy-based approach for network anomaly detection in iot environments. IEEE Access **7**, 169296–169308 (2019)
8. Gupta, B., Badotra, S., Quamara, M., Choudhary, S.: Distributed denial of service attacks detection techniques in cloud computing and iot: Challenges and future directions. Computer Communications **178**, 283–300 (2021). https://doi.org/10.1016/j.comcom.2021.07.017
9. Hamza, A., Gharakheili, H.H., Benson, T.A., Sivaraman, V.: Detecting volumetric attacks on iot devices via sdn- based monitoring of mud activity. In: Proceedings of the 2019 ACM Symposium on SDN Research (SOSR) (2019), https://www.andrew.cmu.edu/user/theophib/papers/SoSR19.pdf
10. Kaynar, B., Sivrikaya, F.: Distributed attack graph generation with deep learning for network security. In: 2019 IEEE Symposium on Computers and Communications (ISCC). pp. 1–6. IEEE (2019)
11. Koroniotis, N., Moustafa, N., Sitnikova, E., Turnbull, B.: Towards the development of realistic botnet dataset in the internet of things for network forensic analytics: Bot-iot dataset. Future Generation Computer Systems **100**, 779–796 (2019)
12. Marcov, L., et al.: Dao–dio routing manipulation dataset (2023). https://doi.org/10.15146/R3K398, https://doi.org/ 10.15146/R3K398
13. Mirsky, Y., et al.: Kitsune Network Attack Dataset – NTP Amplification Subset. https://www.kitsune-dataset. example.org/ntp (2023), accessed 5 May 2025
14. Mirsky, Y., Doitshman, T., Elovici, Y., Shabtai, A.: Kitsune: An ensemble of autoencoders for online network intrusion detection. In: Proceedings of the Network and Distributed System Se- curity Symposium (NDSS). The Internet Society (2018), https://www.ndss-symposium.org/ndss2018/ kitsune-ensemble-autoencoders-online-network-intrusion-detection/
15. Moustafa, N., Turnbull, B., Choo, K.K.R.: An ensemble intrusion detection framework for iot networks using deep learning and feature selection. IEEE Transactions on Industrial Informatics **18**(6), 4022–4031 (2022)
16. Paxson, V., Allman, M., Chu, J., Sargent, M.: Computing TCP's Retransmission Timer. RFC 6298 (2011)
17. Pérez, J., Arenas, M., Gutierrez, C.: Semantics and complexity of sparql. ACM Transactions on Database Systems

34(3), 16:1–16:45 (2009)

18. Raoof, A., Matrawy, A., Lung, C.H.: Routing attacks and mitigation in iot networks: Rpl-based approach. IEEE Internet of Things Journal **7**(8), 7368–7381 (2020). https://doi.org/10.1109/JIOT.2020.2979481
19. Sicari, P., Rizzardi, A., Coen-Porisini, A.: 5g in the internet of things era: An overview on security and privacy challenges. Computer Networks **179**, 107345 (2020). https://doi.org/10.1016/j.comnet.2020.107345
20. Sicari, P., Rizzardi, A., Coen-Porisini, A.: 5g in the internet of things era: An overview on security and privacy challenges. Computer Networks **179**, 107345 (2020). https://doi.org/10.1016/j.comnet.2020.107345
21. Sicari, P., Rizzardi, A., Grieco, L., Coen-Porisini, A.: Security, privacy and trust in internet of things: The road ahead. Computer Networks **76**, 146–164 (2015). https://doi.org/10.1016/j.comnet.2014.11.008
22. Singh, P., Kumar, R., Gupta, S.: Entropy-based cyber threat detection in cloud-iot systems: A review and future directions. Journal of Network and Computer Applications **224**, 103845 (2024)

23. Suryotrisongko, H.W., Akbar, M.: Anomaly detection in internet of things using isolation forest algorithm. In: 2018 International Electronics Symposium (IES). pp. 449–454. IEEE (2018). https://doi.org/10.1109/ELECSYM.2018. 8615532
24. Tosi, D., Pazzi, R.: Design and experimentation of a distributed information retrieval-hybrid architecture in cloud iot data centers. In: IFIP International Internet of Things Conference. pp. 12–21. Springer (2024)
25. Wang, P., Chen, Q., Peng, S.: Graph-based security analysis for industrial control systems. IEEE Transactions on Industrial Informatics **14**(5), 1890–1900 (2018)
26. Wilson, E.: Probable inference, the law of succession, and statistical inference. Journal of the American Statistical Association **22**(158), 209–212 (1927). https://doi.org/10.1080/01621459.1927.10502953
27. Yin, C., Zhu, Y., Fei, J., He, X.: A deep learning approach for intrusion detection using recurrent neural networks. IEEE Access **5**, 21954–21961 (2017). https://doi.org/10.1109/ACCESS.2017.2762418
28. Zaharia, M., Chowdhury, M., Das, T.e.: Resilient distributed datasets: A fault-tolerant abstraction for in-memory cluster computing. In: USENIX NSDI. pp. 15–28 (2012)
29. Zaharia, M., Chowdhury, M., Franklin, M.J., Shenker, S., Stoica, I.: Apache spark: A unified engine for big data processing. Communications of the ACM **59**(11), 56–65 (2016). https://doi.org/10.1145/2934664

Disclaimer/Publisher's Note: The statements, opinions and data contained in all publications are solely those of the individual author(s) and contributor(s) and not of MDPI and/or the editor(s). MDPI and/or the editor(s) disclaim responsibility for any injury to people or property resulting from any ideas, methods, instructions or products referred to in the content.